Information storage in permalloy modulated magnetic nanowires

Guidobeth Sáez (guidobeth.saez@ufrontera.cl)
Universidad de La Frontera
Pablo Díaz
Universidad de La Frontera
Eduardo Cisternas
Universidad de La Frontera
Eugenio E. Vogel
Universidad de La Frontera
Juan Escrig
Universidad de Santiago de Chile (USACH)

Research Article

Keywords: nanometric structures, nanowires, magnetic material, magneto-optoelectronics, magneto-plasmonics

Posted Date: June 17th, 2021

DOI: https://doi.org/10.21203/rs.3.rs-619334/v1

Information storage in permalloy modulated magnetic nanowires

Guidobeth Sáez[1,*], Pablo Díaz[1], Eduardo Cisternas[1], Eugenio E. Vogel[1,2], and Juan Escrig[2,3]

[1]Department of Physics, Universidad de La Frontera, Casilla 54-D, Temuco, Chile
[2]Center of Nanoscience and Nanotechnology (CEDENNA), 9170124, Santiago, Chile
[3]Departamento de Física, Universidad de Santiago de Chile (USACH), Avda. Ecuador 3493, 9170124 Santiago, Chile
[*]guidobeth.saez@ufrontera.cl

ABSTRACT

A long piece of magnetic material shaped as a central cylindrical wire (diameter $d = 50$ nm) with two wider coaxial cylindrical portions (diameter $D = 90$ nm and thickness $t = 100$ nm) defines a bimodulated nanowire. Micromagnetism is invoked to study the equilibrium energy of the system under the variations of the positions of the modulations along the wire. The system can be thought of as composed of 5 independent elements (3 segments and 2 modulations) leading to $2^5 = 32$ different magnetic configurations. We investigate the stability of the configurations depending on the positions of the modulations. The relative chirality of the modulations has negligible contributions to the energy and they have no effect in the stability of the stored configuration. However, the modulations are extremely important in pinning the domain walls that lead to consider each segment as independent from the rest. A phase diagram reporting the stability of the inscribed magnetic configurations is produced. The stability of the system was then tested under the action of external magnetic fields and it is found that more than 50 mT are necessary to alter the inscribed information. The main purpose of this paper is to find weather a prototype like this can complemented to be used as firmware or magnetic keys. Present results indicate that this is feasible.

Introduction

Nanometric materials are not only smaller than their macro counterparts but they also exhibit new properties[1,2]. Among the different nanometric structures, nanowires are the focus of different research groups due to their high aspect ratio, physicochemical properties, together with outstanding mechanical, electrical, magnetic and optical properties, which can also be controlled by varying their geometrical parameters. Furthermore, nanowires are used in many technological applications in different fields like nanoelectronics[3,4], magneto-optoelectronics[5–8], magneto-plasmonics[9] and even in wearable electronic systems[10], among others.

Magnetic nanowires that have a square cross-section are known as planar nanowires and are obtained mainly by lithographic techniques. However, magnetic nanowires with circular cross-section are the ones that concentrate most of the interest today because their curved surface may cause the curvature-induced effective anisotropy or chiral symmetry breaking[11], being used in potential applications[12–14]. Furthermore, cylindrical nanowires favor the formation of unconventional magnetic textures whose dynamics differ considerably from those that appear in two-dimensional wires[15]. In fact, in cylindrical systems Walker breakdown occurs at very high current densities[16] or can even be suppressed[17]; thus, once domain walls are depinned they are expected to move at very high velocities.

In order to synthesize cylindrical nanowires there are mainly two ways: template-free[18,19] or template-assisted[20–22] methods. This last method based on self-organized porous membranes has made notable advances, allowing us to dream of the design proposed by Parkin in 2008 of a racetrack memory[23]. This memory is based on the fact that information can be stored in a solid-state device through magnetic domains (areas where magnetic moments point in a defined direction) separated by magnetic domain walls (areas where magnetic moments vary from the direction of one domain to the other). These domain walls can be moved either by applying an external magnetic field[20,24,25], a spin-polarized current[17], spin waves[26] or localized temperature gradients[27]. The idea is that the position of these magnetic domain walls can be precisely controlled through pinning centers, which can be generated by varying the composition of the nanowire[28–30] or by introducing geometrical inhomogeneities[20,24,31–39], such as modulations in its diameter during the synthesis process. Diameter modulations of the nanowire effectively allow controlling the domain wall positions since they locally reduce the magnetostatic and exchange energy in the different cross-sectional parts[40–48]. Recently, Salem *et al.*[49] went further and succeeded in synthesizing magnetic

nanowire arrays by modulating both their composition and their diameters using a new synthesis method. Although we propose here permalloy as the material of study, this is merely by simplicity, although the search for properties in nanowires of other materials is a very actual research field.[50]

In this article, we assume that diameter modulated nanowires can eventually store firmware. Thus, one of the main goals of the present paper points to recognize the main role of the modulations: Are they simple spacers or could they also be used to store information? Then, we want to study the stability of the inscribed magnetic orientations along the segments (thinner elements between modulations): what are the conditions for a stable inscribed magnetic configuration that does not spontaneously reverses the magnetization in some segments? The robustness of the system will then be tested with respect to externally applied magnetic fields (accidental or intentional). When solving this problem, we will also find some other interesting fundamental features like the presence of Bloch Points (BPs) in some of the configurations. BPs are not an objective of the present paper, but we will just unfold them since they are an intrinsic property of the system proposed here.

Our system then consists of a solid and homogeneous cylindrical piece of magnetic material modulated in diameter along the axis. We assume that modulations are wider in diameter than the central part that is then divided into segments: there are N modulations and $(N+1)$ segments all concentric along the axis. The parameter space includes at least the following geometrical properties: length L of the total nanowire, number of modulations N, thickness of the individual modulations t_i ($i = 1,2,..N$), diameter of the individual modulations D_i ($i = 1,2,..N$), length of the individual segments ℓ_j ($j = 1,2,..N+1$), diameter of the individual segments d_j ($j = 1,2,..N+1$), with only one constraint:

$$\sum_{i=1}^{N} t_i + \sum_{j=1}^{N+1} \ell_j = L. \tag{1}$$

Such complex parameter space necessarily needs to be filtered to focus on the main general properties of the system: the possibility to inscribe a desired magnetic configuration that will be robust enough so it does not reverse spontaneously and it is also stable even when weak or moderate external magnetic fields are applied to it. This task will be done in the next section.

This paper is organized in the following way: Next section describes the system and the methodology; the Third Section is devoted to results and discussions followed by the section with conclusions. Additionally we prepared a separate file with Supporting Information to provide for a wider basis for deeper discussions.

1 System and methodology

1.1 System

Let us consider an isolated permalloy nanowire as illustrated in Fig. 1. We perform our calculations for a device with a representative length $L = 1100\,nm$ with two modulations μ_i ($i = 1,2$) in diameter along its axis, which divide the main nanowire into three segments S_j ($j = 1,2,3$). To further simplify the parameter space, we make all thicknesses (t_i) and diameters (D_i, d_j) the same. Namely, $t_i = t = 100\,nm$; $D_i = D = 90\,nm$ for all i; and $d_j = d = 50\,nm$ for all j. Thus, the only free parameters left are ℓ_1, ℓ_2, and ℓ_3, namely, the lengths of the segments limited by the modulations with the constraint $\ell_1 + \ell_2 + \ell_3 = 900\,nm$. This choice of parameters was motivated by a previous result showing that the coercivity of a monomodulated magnetic nanowire depended strongly on its position along the axis[51].

In general, the aspect ratio between the length and diameter of a ferromagnetic cylinder defines three possible minimum energy configurations: ferromagnetic in-plane (I), ferromagnetic out-of-plane (II) and vortex (III)[52]. If segments are long enough their preferred magnetization will point in any of the two directions along the axis[53]. By a similar token, D and t can be chosen so the dominant magnetization within the modulation (bare disk) is a vortex, where chirality can be clockwise or counterclockwise. To focus on how the geometrical parameters of the system influence its magnetic properties, we consider permalloy nanowires, since this material does not exhibit noticeable crystalline anisotropy[54] like Co[55] or Ni[50] for example .

Although previous set of parameters is a bit arbitrary, it represents the kind of system we are looking for: a simple device with magnetically separate elements capable of storing stable enough magnetic configurations. Variations to these values could modulate the behavior reported below, but the general properties of the device are already established.

1.2 Magnetic configurations

The entire system is composed of 5 elements: three segments and two modulations. This realization should be considered as a first prototype only; from here several variations in the number of modulations and variations of geometrical parameters are possible. Due to shape anisotropy, magnetization in the segments is largely axial with two possible orientations. Similarly, magnetization in the isolated modulations tends to be in the vortex phase with two chirality twists. Altogether there are $2^5 = 32$ independent configurations. A figure in the Supporting Information illustrates each one of these configurations. Due to the symmetry in the Hamiltonian they are doubly degenerate so we need to study the energy of only 16 of them; the other 16 have the same energy as those configurations reached upon reversing every single spin. Moreover, energy difference due to

the different relative chiralities in the modulations turns out to be of the order of 0.01 eV as presented in the second figure of the Supporting Information. Such energy difference is negligible compared to the other energies under consideration here, like the energy difference observed when two contiguous segments have opposite magnetization, which turns out to be of the order of 100 eV. Moreover, such equilibrium energy differences lose significance even when compared to the thermal noise present at normal room temperatures. Thus, we need to consider only 4 independent and energetically different configurations coming from the magnetic orientations along the segments. These four configurations are shown in Fig. 2 for $\ell_1 = 135\ nm$, $\ell_2 = 225\ nm$ and $\ell_3 = 540\ nm$ as an example.

These configurations could be inscribed in the system in different ways. As an example, let us consider configuration C_4 of Fig. 2 to illustrate a possible way of achieving this purpose. Let us expose the entire device to an external strong magnetic field that will orientate all the three segments in the blue direction. Then we approach to the upper end a magnetic field strong enough to reverse the magnetization of that end only. Finally, we do a similar job on the other end reversing that portion from blue to red. Similarly, configurations C_2 and C_3 can be inscribed. Any of these combinations plus the different lengths of the segments can be used to store information in the form of firmware or a magnetic key. The purpose of the rest of the paper is precisely to test the stability of the inscribed information depending on the geometry of the device.

1.3 Geometrical parameter space

The parameter space has only two free variables since the sum of the segments is limited to 900 nm. Let us separate ℓ_2 as a singular variable due to its different role. Then the other two segments can be better considered by their relative lengths in the following way: we define $\zeta = 1 - \frac{\ell_1}{\ell_3}$ for $\ell_1 < \ell_3$ (positive values) and as $\zeta = \frac{\ell_3}{\ell_1} - 1$ for $\ell_3 < \ell_1$ (negative values). If $\zeta = 0$ the segments at the ends have equal length, regardless of the value of ℓ_2; while if $\zeta = +1(-1)$ it implies that the upper (lower) segment does not exist. However, we set a minimum value of 50 nm for either ℓ_1 or ℓ_3 to preserve the axial symmetry in these segments.

For this two-dimensional parameter space, $\{\ell_2, \zeta\}$, we consider that ℓ_2 takes values between 50 nm and 850 nm and ζ takes values between $+0.9$ and -0.9. To optimize the computational time we have considered different steps for ℓ_2 in three ranges: $\ell_2 = 50 - 100$ nm with $\Delta\ell_2 = 10$ nm, $\ell_2 = 100 - 800$ nm with $\Delta\ell_2 = 100$ nm, and $\ell_2 = 800 - 850$ nm with $\Delta\ell_2 = 10$ nm. As will be seen below (Fig. 3), the reason for considering small values in $\Delta\ell_2$, for the first range (small values of ℓ_2) and the third range (large values of ℓ_2), arises from the need to observe in more detail the zones in which the value of ℓ_2 strongly influences the stability of the inscribed magnetic configurations.

1.4 Simulation software and material parameters

To study and understand the stability of the magnetic configurations and the magnetization reversal processes, we have made use of Mumax3 to numerically solve the Landau-Lifshitz-Gilbert equation given by.

$$\frac{d\mathbf{m}}{dt} = -\frac{\gamma_0}{1+\alpha^2}\left[\mathbf{m}\times\mathbf{H}_{eff} + \alpha\mathbf{m}\times(\mathbf{m}\times\mathbf{H}_{eff})\right] \tag{2}$$

where $\mathbf{m}(r,t)$ is the normalized magnetization vector $\mathbf{m}(r,t) = \mathbf{M}(r,t)/M_s$, with M_s as the saturation magnetization, γ_0 is the gyromagnetic ratio and α is the Gilbert damping constant. The equation describes both the precession and relaxation motion of the magnetization in an effective field $\mathbf{H_{eff}}$. For the simulations, we consider permalloy as the material with its properties represented by the following parameters: saturation magnetization of $M_s = 800 \times 10^3$ A/m and stiffness constant of $A = 13 \times 10^{-12}$ J/m[51]. We have used cell sizes of $2 \times 2 \times 2$ nm^3. Besides, the damping constant is chosen to a fix value of $\alpha = 0.5$.

One of the main objectives of the present work is to evaluate the stability of the inscribed magnetic configurations, analyzing possible spontaneous reversals of the magnetization. In solving the LLG equation in time, starting from some initially incribed configurations of the magnetization, we have applied a cutoff criterion on the torque given by:

$$\frac{\tau_{max}}{\gamma_0} = \frac{1}{\gamma_0}\max\left(\frac{d\mathbf{m}_i}{dt}\right) \tag{3}$$

where $d\mathbf{m}_i/dt$ is given by Eq. 2 and $\mathbf{m}_i$ is the magnetization of the i-th cell. In our case, we have considered the following as the cutoff criteria $\tau_{max}/\gamma_0 = 10^{-4}$ T.

2 Results and discussions

The relative chirality of the modulations plays a negligible role in the equilibrium energy as shown in Fig. 2 of the SI. Thus, such energy is low, of the order to 0.01 eV for the example in the figure and it remains within this order of magnitude for the

configurations studied here. However, for configurations with different orientation between segments, the energy differences are of the order of 80 eV (see Fig. 3 of SI). So, for this system, more than three orders of magnitude separate the energy differences due to modulation interactions from segments interactions.

Next illustrative result is given in Fig. 2 where the 4 independent magnetic configurations C_1, C_2, C_3 and C_4, left after neglecting the interactions between modulations are shown. C_1: the three segments present parallel magnetization; C_2: the shorter external segment presents opposite magnetization with respect to the other two segments; C_3: the longer external segment presents opposite magnetization with respect to the other two segments; C_4: the internal segment presents magnetization opposed to the other two segments. The equilibrium energy of each configuration E_1 through E_4 is given underneath: it increases in the same order of previous presentation. However, the difference between C_2 and C_3 is of only 2 eV while the other differences are almost a hundred eV. This is directly related to the number of domain walls pinned within the modulations. A more complete picture is given in Fig. 5 in the SI.

How stable are these configurations with respect to the position of the modulations? Namely, if the magnetization orientation defining each configuration is inscribed in the device, will it remain so or will it spontaneously decay to a lower energy configuration? To answer this question, we have prepared a phase diagram in Fig. 3.

The common abscissa axis in Fig. 3 gives the length ℓ_2 in *nm* of the central segment; the ordinates give the proportion in which ℓ_1 and ℓ_3 are present according to the ζ parameter defined in the subsection "Geometrical parameter space". Each pixel here corresponds to an independent micromagnetic simulation as described in methodology.

Panel (a) corresponds to initializations with C_1 configuration that is the true ground configuration so it cannot change. However some of the pixels present configurations with higher energies around $\zeta = 0$ and $\ell_2 \approx 810\,nm$. Panel (b) represents final states reached by systems initiated as C_2. Although most of the parameter space represents stability, those configurations with large enough ℓ_2 combined with moderate to large values of $|\zeta|$ are unstable and decay to C_1 as revealed by the color code. It can be noticed that even for some of the borderline configurations remaining as C_2 the energy decreases evidencing the onset for the decay conditions. Panel (c) corresponds to initiations with C_3 configuration; the analysis here is identical to previous one due to the symmetry $\zeta \to -\zeta$ conserving ℓ_2 that takes C_2 into C_3. Panel (d) corresponds to configurations initiated as C_4 that can decay to C_2 and C_3 for $|\zeta|$ over a minimum determined by ℓ_2, which also must be large enough. Moreover, if ℓ_2 is too large the system initiated as C_4 can decay directly into a C_1 configuration. All of this is conveniently presented by means of color codes and height of the energy column.

The phase diagram presented in Fig. 3 has been built around the parameter space arising from the system defined in Fig. 1 with the geometrical values valid for the prototype defined above. In case a different geometry is needed the same procedure can be applied to find the stability regions of the desired magnetic configuration storing the information that needs to be protected from spontaneous erasure.

But information can also be lost if an external magnetic field comes close to the system and reverses the magnetization in one or more segments. How strong this magnetic fields needs to be? To answer this question for a representative case we present in Fig. 4 the exposition of C_4 to an external magnetic field along the z direction since this would be the most effective way to reverse the magnetization in the segments thus altering the stored information. Panel (a) presents the case for a constant and uniform magnetic field beginning at zero and increasing its magnitude in the negative z direction, while panel (b) does the same but along the positive z direction opposite to the magnetization of segment S_2. Let us consider the latter first due to its simplicity: the magnetization grows slightly due mainly to polarization within the modulations; actually BPs tend to get closer to each other. When the magnetic field reaches a value close to $56\,mT$ segment S_2 reverses its magnetization and the system switches to a C_1 configuration in an irreversible way.

The increase of the magnetic field towards negative values, namely along the magnetization of the central segment S_2 is more complex than previous one. The shorter end segment reverses its magnetization at a field of $-49\,mT$ switching the configuration to C_3 in an irreversible way. If the intensity of the field continues to increase the configuration changes to C_1 at a field of about $-59\,mT$ in an irreversible way.

These critical fields can be improved a bit upon choosing the lengths of the segments in a more appropriate way. However, the order of magnitude corresponds to the one given in this example, which is more than three orders of magnitude over the average Earth magnetic field. In any case this is a rather high value of a magnetic field for a random contact to a magnetic source. So the system will be robust in most cases where normal magnetic sources are around. Eventually an intentional approach by a very strong permanent magnet in the appropriate direction could damage the stored information. Other than such sabotage attacks this system offers the possibility of storing firmware or magnetic keys in a durable way.

3 Conclusions

A bimodulated cylindrical nanowire can store coded information by means of independent magnetic orientations stored on each of its segments. This was studied here for a prototype but it can be extended to larger systems with more modulations. There seems to be no difficulties in realizing these systems in the laboratory.

Magnetization on short modulations tends to be chiral, however the relative vortex orientations do not play a significant role in the equilibrium energy so the modulations act basically as separators of segments with independent magnetic orientations.

Modulations pin domain walls separating segments with opposite magnetization thus defining sectors of the device where inscribed magnetization is stable under certain geometrical conditions and eventual presence of external magnetic fields.

The domain wall inside the modulation separating segments of different magnetic orientation takes the conic form typical of BPs. This is by itself an interesting problem that we pose here for future developments.

Thermal excitation at room temperature of the order of few meV is far from removing the BPs which requires dozens of eV to be overturned as shown by the simulations reported in this paper.

For each general geometry a phase diagram similar to the one produced here can be obtained to optimize the stability of the inscribed information. This can lead to properly designing a coded bar storing firmware of coded information. Magnetic keys could be constructed in this way not only at the nanoscale but at the microscale also.

External magnetic fields of a few dozen mT are necessary to remove the BPs thus altering the original magnetic configuration stored in the system. Such fields are not randomly available so a device based on this way of storing codes or a magnetic key produced in this way can be very robust.

References

1. Fernández-Pacheco, A. *et al.* Three-dimensional nanomagnetism. *Nat. Commun.* **8**, DOI: 10.1038/ncomms15756 (2017).
2. Sander, D. *et al.* The 2017 magnetism roadmap. *J. Phys. D: Appl. Phys.* **50**, 363001, DOI: 10.1088/1361-6463/aa81a1 (2017).
3. Ferry, D. K. Nanowires in nanoelectronics. *Science* **319**, 579–580, DOI: 10.1126/science.1154446 (2008).
4. Zhou, W. *et al.* Long term stability of nanowire nanoelectronics in physiological environments. *Nano Lett.* **14**, 1614–1619, DOI: 10.1021/nl500070h (2014).
5. Li, Y., Qian, F., Xiang, J. & Lieber, C. M. Nanowire electronic and optoelectronic devices. *Mater. Today* **9**, 18–27, DOI: 10.1016/s1369-7021(06)71650-9 (2006).
6. Lavrijsen, R. *et al.* Magnetic ratchet for three-dimensional spintronic memory and logic. *Nature* **493**, 647–650, DOI: 10.1038/nature11733 (2013).
7. Liu, Q. *et al.* Enhanced magneto-optical effects in composite coaxial nanowires embedded with ag nanoparticles. *Sci. Reports* **6**, DOI: 10.1038/srep29170 (2016).
8. Wagner, M. F. P., Völklein, F., Reith, H., Trautmann, C. & Toimil-Molares, M. E. Fabrication and thermoelectrical characterization of three-dimensional nanowire networks. *physica status solidi (a)* **213**, 610–619, DOI: 10.1002/pssa.201532616 (2016).
9. Valente, J., Ou, J.-Y., Plum, E., Youngs, I. J. & Zheludev, N. I. A magneto-electro-optical effect in a plasmonic nanowire material. *Nat. Commun.* **6**, DOI: 10.1038/ncomms8021 (2015).
10. Gong, S. & Cheng, W. One-dimensional nanomaterials for soft electronics. *Adv. Electron. Mater.* **3**, 1600314, DOI: 10.1002/aelm.201600314 (2016).
11. Gaididei, Y., Kravchuk, V. P. & Sheka, D. D. Curvature effects in thin magnetic shells. *Phys. Rev. Lett.* **112**, DOI: 10.1103/physrevlett.112.257203 (2014).
12. Mourachkine, A., Yazyev, O. V., Ducati, C. & Ansermet, J.-P. Template nanowires for spintronics applications: Nanomagnet microwave resonators functioning in zero applied magnetic field. *Nano Lett.* **8**, 3683–3687, DOI: 10.1021/nl801820h (2008).
13. Kou, X. *et al.* Memory effect in magnetic nanowire arrays. *Adv. Mater.* **23**, 1393–1397, DOI: 10.1002/adma.201003749 (2011).
14. Contreras, M., Sougrat, R., Zaher, A., Ravasi, T. & Kosel, J. Non-chemotoxic induction of cancer cell death using magnetic nanowires. *Int. J. Nanomedicine* 2141, DOI: 10.2147/ijn.s77081 (2015).
15. Burn, D. M., Arac, E. & Atkinson, D. Magnetization switching and domain-wall propagation behavior in edge-modulated ferromagnetic nanowire structures. *Phys. Rev. B* **88**, DOI: 10.1103/physrevb.88.104422 (2013).
16. Otálora, J. A., López-López, J. A., Núñez, A. S. & Landeros, P. Domain wall manipulation in magnetic nanotubes induced by electric current pulses. *J. Physics: Condens. Matter* **24**, 436007, DOI: 10.1088/0953-8984/24/43/436007 (2012).
17. Yan, M., Kákay, A., Gliga, S. & Hertel, R. Beating the walker limit with massless domain walls in cylindrical nanowires. *Phys. Rev. Lett.* **104**, DOI: 10.1103/physrevlett.104.057201 (2010).

18. Athanassiou, E. K., Grossmann, P., Grass, R. N. & Stark, W. J. Template free, large scale synthesis of cobalt nanowires using magnetic fields for alignment. *Nanotechnology* **18**, 165606, DOI: 10.1088/0957-4484/18/16/165606 (2007).

19. Liu, C. *et al.* Template free and binderless NiO nanowire foam for li-ion battery anodes with long cycle life and ultrahigh rate capability. *Sci. Reports* **6**, DOI: 10.1038/srep29183 (2016).

20. Pitzschel, K. *et al.* Magnetic reversal of cylindrical nickel nanowires with modulated diameters. *J. Appl. Phys.* **109**, 033907, DOI: 10.1063/1.3544036 (2011).

21. Col, S. D., Darques, M., Fruchart, O. & Cagnon, L. Reduction of magnetostatic interactions in self-organized arrays of nickel nanowires using atomic layer deposition. *Appl. Phys. Lett.* **98**, 112501, DOI: 10.1063/1.3562963 (2011).

22. Zaraska, L., Jaskuła, M. & Sulka, G. D. Porous anodic alumina layers with modulated pore diameters formed by sequential anodizing in different electrolytes. *Mater. Lett.* **171**, 315–318, DOI: 10.1016/j.matlet.2016.02.113 (2016).

23. Parkin, S. S. P., Hayashi, M. & Thomas, L. Magnetic domain-wall racetrack memory. *Science* **320**, 190–194, DOI: 10.1126/science.1145799 (2008).

24. Berganza, E., Bran, C., Jaafar, M., Vázquez, M. & Asenjo, A. Domain wall pinning in FeCoCu bamboo-like nanowires. *Sci. Reports* **6**, DOI: 10.1038/srep29702 (2016).

25. Col, S. D. *et al.* Nucleation, imaging, and motion of magnetic domain walls in cylindrical nanowires. *Appl. Phys. Lett.* **109**, 062406, DOI: 10.1063/1.4961058 (2016).

26. Kim, S.-K., Lee, K.-S. & Han, D.-S. A gigahertz-range spin-wave filter composed of width-modulated nanostrip magnonic-crystal waveguides. *Appl. Phys. Lett.* **95**, 082507, DOI: 10.1063/1.3186782 (2009).

27. Moretti, S., Raposo, V., Martinez, E. & Lopez-Diaz, L. Domain wall motion by localized temperature gradients. *Phys. Rev. B* **95**, DOI: 10.1103/physrevb.95.064419 (2017).

28. Palmero, E. M., Béron, F., Bran, C., del Real, R. P. & Vázquez, M. Magnetic interactions in compositionally modulated nanowire arrays. *Nanotechnology* **27**, 435705, DOI: 10.1088/0957-4484/27/43/435705 (2016).

29. Berganza, E. *et al.* Multisegmented nanowires: a step towards the control of the domain wall configuration. *Sci. Reports* **7**, DOI: 10.1038/s41598-017-11902-w (2017).

30. Méndez, M. *et al.* Ni-co alloy and multisegmented ni/co nanowire arrays modulated in composition: Structural characterization and magnetic properties. *Crystals* **7**, 66, DOI: 10.3390/cryst7030066 (2017).

31. Pitzschel, K. *et al.* Controlled introduction of diameter modulations in arrayed magnetic iron oxide nanotubes. *ACS Nano* **3**, 3463–3468, DOI: 10.1021/nn900909q (2009).

32. Esmaeily, A. S., Venkatesan, M., Razavian, A. S. & Coey, J. M. D. Diameter-modulated ferromagnetic CoFe nanowires. *J. Appl. Phys.* **113**, 17A327, DOI: 10.1063/1.4794722 (2013).

33. Iglesias-Freire, Ó. *et al.* Spin configuration in isolated FeCoCu nanowires modulated in diameter. *Nanotechnology* **26**, 395702, DOI: 10.1088/0957-4484/26/39/395702 (2015).

34. Palmero, E. M., Bran, C., del Real, R. P. & Vázquez, M. Synthesis and magnetism of modulated FeCo-based nanowires. *J. Physics: Conf. Ser.* **755**, 012001, DOI: 10.1088/1742-6596/755/1/012001 (2016).

35. P, V. M. & Kumar, P. A. Chirality dependent pinning and depinning of magnetic vortex domain walls at nano-constrictions. *J. Magn. Magn. Mater.* **422**, 419–424, DOI: 10.1016/j.jmmm.2016.09.004 (2017).

36. Biziere, N. *et al.* Synthesis and magnetic reversal of bi-conical ni nanostructures. *J. Appl. Phys.* **110**, 063906, DOI: 10.1063/1.3638072 (2011).

37. Palmero, E. M., Bran, C., del Real, R. P. & Vázquez, M. Vortex domain wall propagation in periodically modulated diameter FeCoCu nanowire as determined by the magneto-optical kerr effect. *Nanotechnology* **26**, 461001, DOI: 10.1088/0957-4484/26/46/461001 (2015).

38. Rodríguez, L. A. *et al.* Quantitative nanoscale magnetic study of isolated diameter-modulated FeCoCu nanowires. *ACS Nano* **10**, 9669–9678, DOI: 10.1021/acsnano.6b05496 (2016).

39. Méndez, M. *et al.* Effect of sharp diameter geometrical modulation on the magnetization reversal of bi-segmented FeNi nanowires. *Nanomaterials* **8**, 595, DOI: 10.3390/nano8080595 (2018).

40. Bruno, P. Geometrically constrained magnetic wall. *Phys. Rev. Lett.* **83**, 2425–2428, DOI: 10.1103/physrevlett.83.2425 (1999).

41. Allende, S., Altbir, D. & Nielsch, K. Magnetic cylindrical nanowires with single modulated diameter. *Phys. Rev. B* **80**, DOI: 10.1103/physrevb.80.174402 (2009).

42. Allende, S. & Arias, R. Transverse domain wall propagation in modulated cylindrical nanostructures and possible geometric control. *Phys. Rev. B* **83**, DOI: 10.1103/physrevb.83.174452 (2011).

43. Fangohr, H., Chernyshenko, D. S., Franchin, M., Fischbacher, T. & Meier, G. Joule heating in nanowires. *Phys. Rev. B* **84**, DOI: 10.1103/physrevb.84.054437 (2011).

44. Salem, M. S. *et al.* Magnetic properties of cylindrical diameter modulated ni80fe20 nanowires: interaction and coercive fields. *Nanoscale* **5**, 3941, DOI: 10.1039/c3nr00633f (2013).

45. Tejo, F., Vidal-Silva, N., Espejo, A. P. & Escrig, J. Angular dependence of the magnetic properties of cylindrical diameter modulated ni80fe20 nanowires. *J. Appl. Phys.* **115**, 17D136, DOI: 10.1063/1.4865777 (2014).

46. Sturma, M., Toussaint, J.-C. & Gusakova, D. Geometry effects on magnetization dynamics in circular cross-section wires. *J. Appl. Phys.* **117**, 243901, DOI: 10.1063/1.4922868 (2015).

47. Arzuza, L. *et al.* Domain wall propagation tuning in magnetic nanowires through geometric modulation. *J. Magn. Magn. Mater.* **432**, 309–317, DOI: 10.1016/j.jmmm.2017.01.071 (2017).

48. Fernandez-Roldan, J. A. *et al.* Modeling magnetic-field-induced domain wall propagation in modulated-diameter cylindrical nanowires. *Sci. Reports* **9**, DOI: 10.1038/s41598-019-40794-1 (2019).

49. Salem, M. S. *et al.* Composition and diameter modulation of magnetic nanowire arrays fabricated by a novel approach. *Nanotechnology* **29**, 065602, DOI: 10.1088/1361-6528/aaa095 (2018).

50. Proenca, M. P., Rial, J., Araujo, J. P. & Sousa, C. T. Magnetic reversal modes in cylindrical nanostructures: from disks to wires. *Sci. Reports* **11**, DOI: 10.1038/s41598-021-89474-z (2021).

51. Sáez, G. *et al.* Tuning the coercive field by controlling the magnetization reversal process in permalloy modulated nanowires. *J. Magn. Magn. Mater.* **512**, 167045, DOI: 10.1016/j.jmmm.2020.167045 (2020).

52. Díaz, P., Vogel, E. E. & Munoz, F. Magnetic phases at the molecular scale: the case of cylindrical co nanoparticles. *J. Nanoparticle Res.* **19**, DOI: 10.1007/s11051-017-3879-6 (2017).

53. Metlov, K. L. & Guslienko, K. Y. Stability of magnetic vortex in soft magnetic nano-sized circular cylinder. *J. Magn. Magn. Mater.* **242-245**, 1015–1017, DOI: 10.1016/s0304-8853(01)01360-9 (2002).

54. Kateb, M., Gudmundsson, J. T. & Ingvarsson, S. Effect of atomic ordering on the magnetic anisotropy of single crystal ni80fe20. *AIP Adv.* **9**, 035308, DOI: 10.1063/1.5088602 (2019).

55. Cho, J. U. *et al.* Control of magnetic anisotropy of co nanowires. *J. Magn. Magn. Mater.* **303**, e281–e285, DOI: 10.1016/j.jmmm.2006.01.082 (2006).

Acknowledgements

This work was partially supported by Basal Project Cedenna [ANID grant number AFB180001] and Fondecyt [grant numbers 1190036, and 1200302].

Author contributions statement

G.S was present in every aspect of the present paper, from the calculations, and simulations to the manufacture of the plots, discussions writing and revision of the M.S. P.D contributed to the discussion, plots, and writing. EC contributed to the methodology, analysis and discussions. E.E.V proposed the problem and participated in all aspects G.S did. J.E proposed alternatives to the original development, participated in the discussions, writing of the paper, and revision of the plots and analysis. All the five members were engaged in the final writing of the paper, its revision and approved this final version.

Additional information

The authors declare no competing insterest.

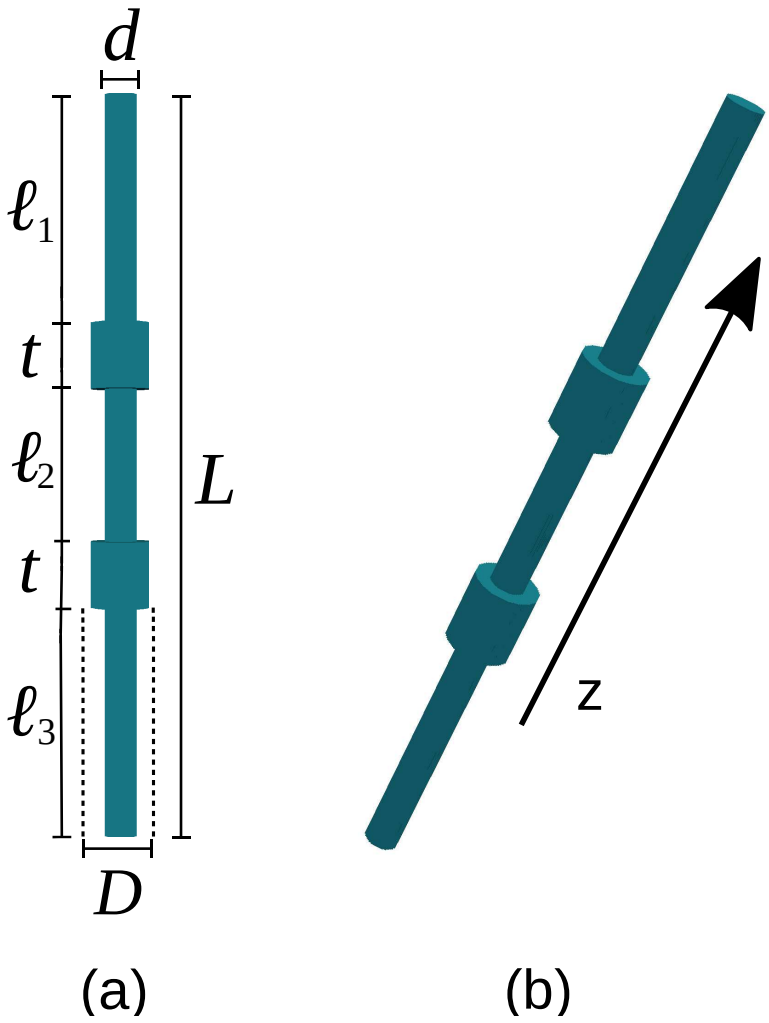

Figure 1. (a) Front view of the proposed bimodulated nanowire with the definition of its geometrical parameters. (b) 3D view of the system where its symmetry axis is parallel to the z-axis along which a magnetic field will be later applied

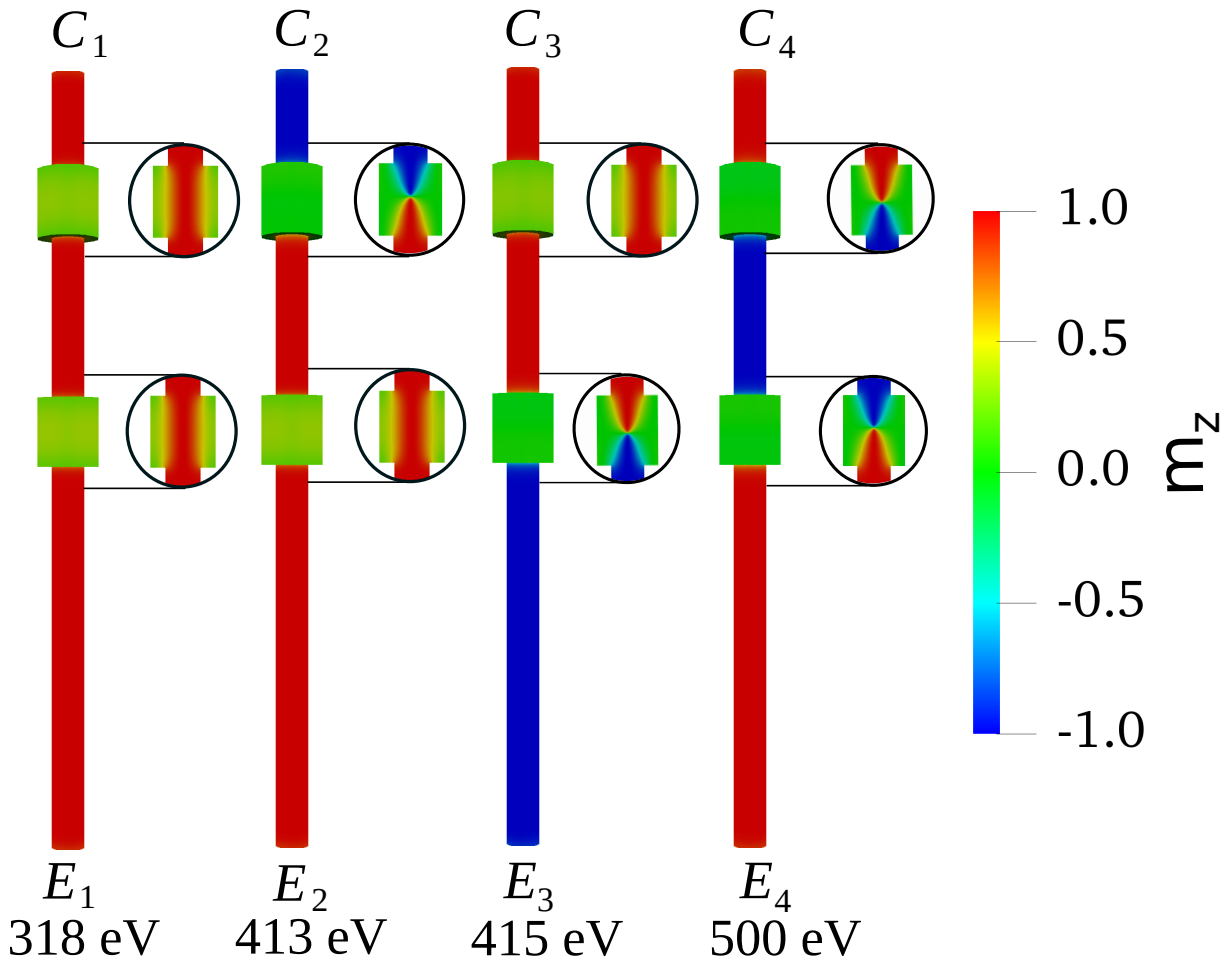

Figure 2. The final 4 energetically distinguishable magnetic configurations in order of increasing equilibrium energy. Magnetization values are illustrated by a color code defined to the right. The shape of the domain walls inside the modulations are shown by circled cuts to the right; when they host end of segments with different orientations BPs naturally appear and they can be recognized by their conical shape.

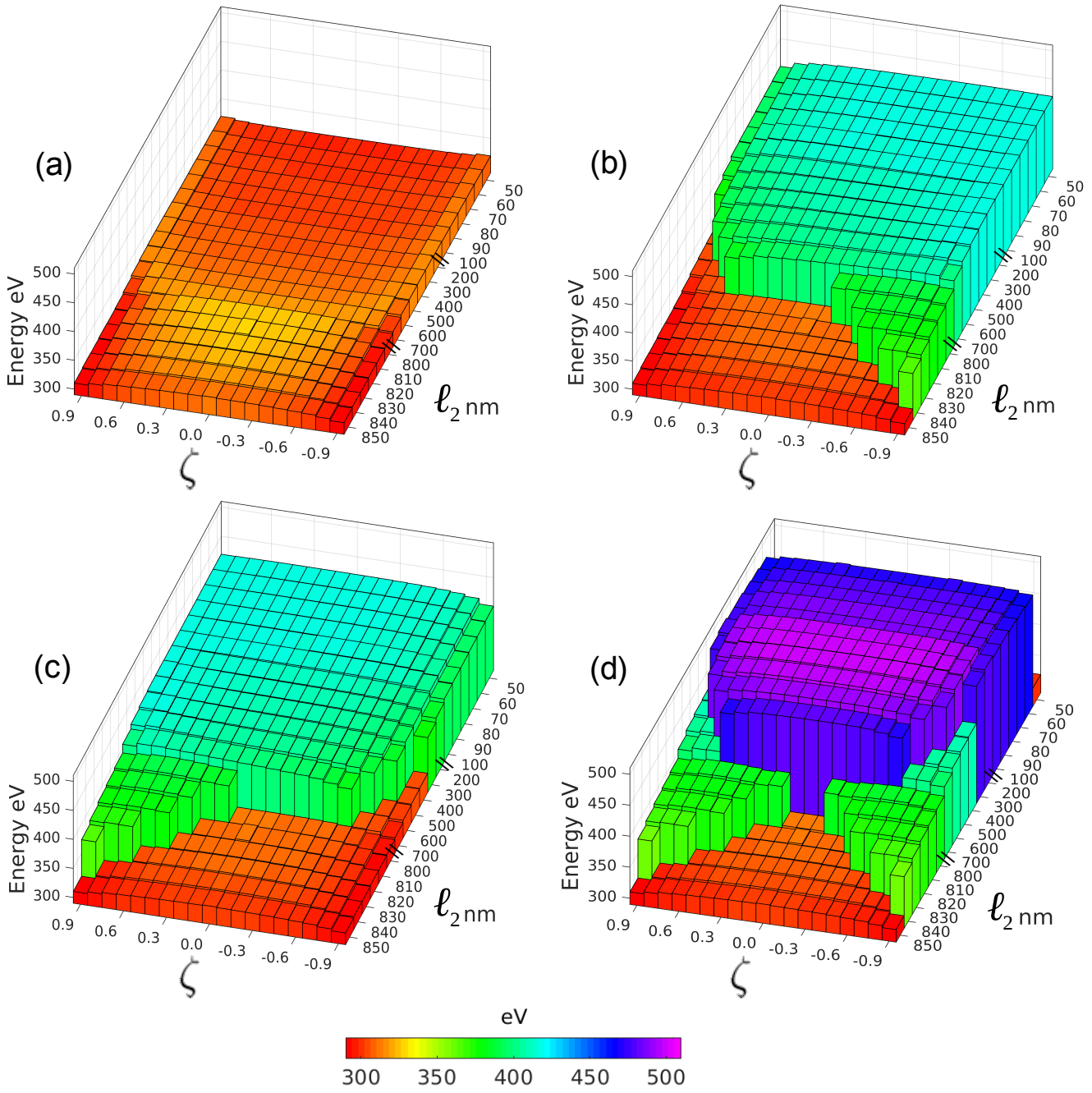

Figure 3. Energy phase diagram testing stability of the inscribed information. Each pixel represents a different ℓ_1, ℓ_2 and ℓ_3 (through ζ) choice and the height gives the corresponding equilibrium or final energy. Panel (a) illustrates the equilibrium energy for an original configuration C_1 inscribed in the system: obviously here it remains in the true ground C_1 configuration although the final energy landscape is not flat. Panel (b) corresponds to a C_2 configuration initially inscribed in the system represented by light gray (blue/green) color; however, for some geometries this initial configuration is unstable and decays to C_1 represented by the corresponding gray (orange) color and lower energies. Panel (c), with C_3 originally inscribed, is symmetric to panel (b) with respect to the sign of ζ. Panel (d) represents systems initiated as C_4 configuration; those remaining as C_4 are marked in dark gray (blue/violet), but some of them are not stable and spontaneously decay to C_2 or C_3 for large enough ℓ_2 values and not very small $|\zeta|$ as represented by light gray color (blue/green); configurations with both large values of ℓ_2 and small $|\zeta|$ can collapse directly into C_1 configurations as presented by pixels in gray (orange) color.

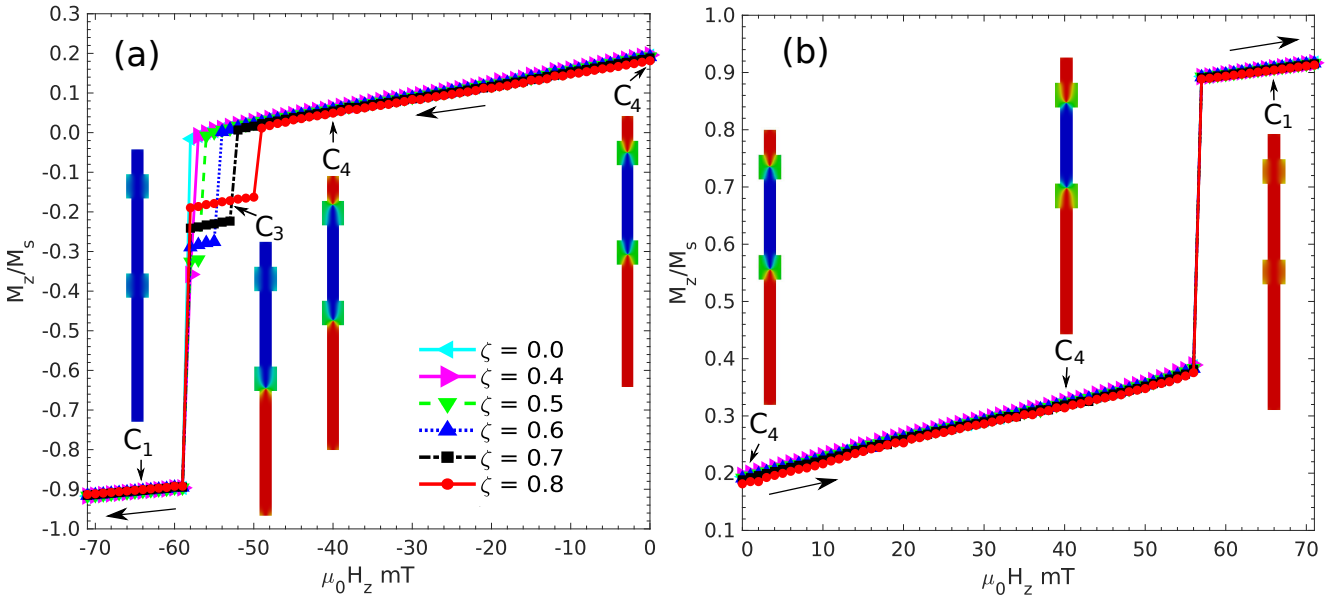

Figure 4. Magnetization curves for an initial C_4 configuration and a varying external constant and uniform magnetic field applied in a negative (a) and positive (b) direction along the z-axis. In this representative example $\ell_2 = 300\,nm$ and different ζ values are considered as given in the inset. Illustration of the magnetization (using the same color code as before) in the system are given at representative field values

Supplementary Files

This is a list of supplementary files associated with this preprint. Click to download.

- PAPERBIMODULATEDSI.pdf